Journal of Materials Chemistry A

PAPER

View Article Online
View Journal | View Issue

Cite this: J. Mater. Chem. A, 2014, 2, 19797

Centrifugation-free and high yield synthesis of nanosized H-ZSM-5 and its structure-guided aromatization of methanol to 1,2,4-trimethylbenzene†

Kui Shen,[ab] Weizhong Qian,*[a] Ning Wang,[a] Chang Su[a] and Fei Wei[a]

Nanosized H-ZSM-5 has been proven to be an efficient way to improve mass transport properties with shape selectivity in many catalytic reactions. Generally, the synthesis of very fine nanosized H-ZSM-5 always suffers from low product yield and requires a complicated centrifugal separation process, both of which severely hinder its large-scale preparation and industrial applications. Herein, we report a centrifugation-free and high yield synthesis route for hierarchically nanosized ZSM-5 with a wide Si/Al ratio range by a combination of pre-aging process and steam-assisted conversion method using alkalis-free powder as the ZSM-5 precursor. This facile route not only avoids the energy-intensive centrifugal separation and ion-exchange process, but also significantly increases the crystallization efficiency along with a high yield. The obtained nanosized ZSM-5 possesses an ultrafine uniform size, high surface area, high total pore volumes, tunable Si/Al molar ratio, and high crystallinity. As a result, the nanosized ZSM-5 shows excellent catalytic performance when used in the catalytic conversion of methanol to aromatics. Notably, the nanosized ZSM-5 with a Si/Al_{th} of 60 (NZS-60) shows an almost 25-fold longer catalytic lifetime, as well as up to 16% higher total aromatic selectivity when compared with conventional ZSM-5. Furthermore, the selectivity of 1,2,4-trimethylbenzene over this catalyst can be up to 44% in all products and 64% in aromatics products. Characterization results of the spent samples reveal that the most-improved catalytic performance and high selectivity of 1,2,4-trimethylbenzene over the nanosized ZSM-5 could be attributed to its small crystal size and hierarchical structure, which not only prevents the deposition of polyaromatic hydrocarbon in the microspores, but also sharply increases the reaction efficiency of bulky intermediate products on the surface of the catalyst.

Received 28th August 2014
Accepted 6th October 2014

DOI: 10.1039/c4ta04444d

www.rsc.org/MaterialsA

1. Introduction

The limited availability of crude oil stimulates the study of new processes using other cheap or renewable resources to prepare aromatics,[1–7] which are one of the most important raw materials for chemical industry and are basically produced by petrochemical processes such as reforming and cracking using crude oil.[5,8,9] Among the alternative processes, the catalytic conversion of methanol to aromatics (MTA) is a promising technology for the production of high quality aromatics, and thus has attracted extensive attention.[10–12] ZSM-5 zeolite with a MFI structure has been proved to be a highly effective catalyst for the aromatization of a wide range of feedstocks, because of its well-defined channels, high surface area, tunable acidity, and high hydrothermal stability.[2,5,7,13–15] The ZSM-5 zeolite has unique molecular-sized micropores with sinusoidal channels of 0.55 nm × 0.51 nm in [100], and straight channels of 0.56 nm × 0.53 nm in [010], and thus shows excellent shape selectivity in many aromatization reactions.[2,5,7,16,17] However, these definite micropores could cause severe diffusion resistance of larger molecules in the zeolite, and thus often result in quick deactivation by the deposition of carbonaceous residues that block the reactants from accessing the active sites.[13,14,18–20] Nanosized ZSM-5 zeolite has a short channel in all *a*, *b*, *c*-axis directions and allows the quick diffusion of reactants or intermediate products, and consequently exhibits a much longer lifetime in high temperature catalytic processes, compared to conventional microsized ZSM-5. However, the annual amount of nanosized ZSM-5 produced to date is far lower than that of microsized ZSM-5, due to the following apparent engineering challenges. First, the traditional synthesis routes for nanosized ZSM-5, mainly concentrating on the confined space synthesis[21–26] and clear solutions synthesis,[27–30] are normally conducted in

[a]Beijing Key Laboratory of Green Chemical Reaction Engineering and Technology, Department of Chemical Engineering, Tsinghua University, Beijing 100084, P.R. China. E-mail: qianwz@tsinghua.edu.cn

[b]School of Chemistry and Chemical Engineering, South China University of Technology, Guangzhou 510640, P.R. China

† Electronic supplementary information (ESI) available. See DOI: 10.1039/c4ta04444d

aqueous solutions with NaOH as the mineralizer.[21,22] Thus, the as-prepared nanosized Na-ZSM-5 in crystallization liquids always requires repeated energy-intensive centrifugal separation and an ion-exchange process to obtain the final active H-form nanosized ZSM-5. The significant energy consumption and long-time operation seriously retard its commercial application. Second, the hydrothermal synthesis of nanosized ZSM-5 always suffers from low product yield, and thus results in stringent environmental regulations due to the uncrystallized aluminosilicate and serious loss of centrifugal separation in the remaining synthesis solution.[27,29,31,32] It is, therefore, highly desirable to develop a novel route for nanosized H-ZSM-5 in terms of simplicity, reproducibility, and large-scale applicability for the MTA process.

Herein, we report a centrifugation-free and high yield route for nanosized H-ZSM-5 with excellent structural properties by a combination of pre-aging process and steam-assisted conversion (SAC) method using alkalis-free powder as the ZSM-5 precursor. The thorough characterization and systematic study of the synthesis conditions indicate that the nanosized ZSM-5 with an ultrafine size (30–60 nm), wide Si/Al ratio range, high surface area (above 440 $m^2\ g^{-1}$), high total pore volumes (above 0.7 $cm^3\ g^{-1}$), and high crystallinity can be obtained by a two-step approach with an aging time of 72 h in 90 °C and an NH_4NO_3/SiO_2 molar ratio of 0.017–0.34. Then, these obtained nanosized ZSM-5 catalysts with different densities of acid sites (Si/Al_{th} = 30, 60 and 90) were applied as a solid acid catalyst for the catalytic conversion of methanol to aromatics. The reaction results indicate that the nanosized ZSM-5 has a much better catalytic stability and higher selectivity of 1,2,4-trimethylbenzene compared to conventional ZSM-5. To determine the reason, we thoroughly studied the deactivated catalysts and monitored the quantity and location of coke formation during the reaction.

2. Experimental section

2.1. Centrifugation-free and high yield synthesis of nanosized ZSM-5

The reactants used in the synthesis were tetraethylorthosilicate (TEOS, Beijing Modern Eastern Fine Chemicals Co., Ltd), tetrapropylammonium hydroxide (TPAOH, 25% in water, Zhejiang Ken Te Chemical Co., Ltd.), Aluminium nitrate nonahydrate ($Al(NO_3)_3\cdot 9H_2O$, Beijing Chemical Works) and ammonium nitrate (NH_4NO_3, Beijing Chemical Works).

In this study, three samples with Si/Al_{th} molar ratios of 30, 60 and 90 (denoted as NZS-30, NZS-60 and NZS-90) were synthesized using this facile synthesis route to certify the tunable Si/Al of our route to cater the strict operation condition of the MTA reaction. In a typical synthesis of nanosized ZSM-5, 24.3 g TEOS, used as the silica source, was added into 25.8 g TPAOH with continuous stirring. The molar composition of the gel was $92SiO_2 : 25TPAOH : 479H_2O : 368EtOH$. The presence of ethanol (EtOH) in the mixed gel was due to the hydrolysis of TEOS with H_2O. After homogenizing at room temperature for 1 h, the mixture was hydrothermally treated at 90 °C for 72 h. After cooling down, the solution containing a little water, 0.58–1.43 g $Al(NO_3)_3\cdot 9H_2O$, and 0–0.75 g NH_4NO_3 was slowly added to the mixture. The resulting mixture was further stirred for about 1 h, and then heated at 60 °C to complete dryness. The resulting dry precursor lumps were coarsely crushed. Then, 5 g of precursor powder was transferred into a 15 mL Teflon cup, which itself was placed into a 70 mL Teflon liner with a support. 2 g of distilled water was poured at the bottom of the liner without contacting the dry gel in the inner Teflon cup. The charged liner assembly was placed into an 80 mL steel reactor and transferred into a preheated oven at 180 °C and heated for 24 h. The crystallization reaction was subsequently quenched by cold water. The obtained powder was directly dried at 110 °C overnight, without centrifugal separation and ion-exchange steps, and subsequently calcined in air at 550 °C for 5 h to remove the template (TPAOH) to obtain the final H-form nanosized ZSM-5.

For comparison, three conventional Na-ZSM-5 with Si/Al_{th} of 30, 60, and 90 (Fig. S2†) were also synthesized according to the method reported by JC Groen *et al.*,[33] but with a slight modification. The corresponding H-ZSM-5 (denoted as CZS-30, CZS-60 and CZS-90, respectively) were prepared through ion-exchange three times and *via* calcination with conventional Na-ZSM-5 as the starting material. As detailed, the obtained conventional Na-ZSM-5 was first converted to the ammonium form by cation-exchange in a NH_4NO_3 solution. Five grams of Na-ZSM-5 was dispersed in 100 mL NH_4NO_3 solution (1 M) and vigorously stirred for 6 h. The solid products were collected by filtering separation. The exchange process was performed repeatedly for 3 times to complete the exchange reaction, and NH_4-ZSM-5 was formed. The final C-ZSM-5 product was obtained by calcining the NH_4-ZSM-5 powder at 550 °C for 5 h. In order to investigate the necessity of the cation-exchange process, the N-ZSM-5 obtained directly by the direct synthesis route was also ion-exchanged according to the process above, except the use of centrifugal separation with a high speed of 12 000 rpm for 30 min.

2.2. Characterization of the fresh ZSM-5 samples

X-ray diffractions (XRD) were recorded with a Rigaku D/Max-RB diffractometer using Cu Kα Radiation at 40 kV and 120 mA. Scanning electron microscopy (SEM) images were performed by a high-resolution scanning electron microscope (JEOL, JSM-7401) at 3.0 kV. TEM experiments were performed on a high-resolution transmission electron microscope (JEOL, JEM-2010, exited at 120 kV). Brunauer–Emmett–Teller (BET) surface area were recorded in a Quantachrome automated surface area and porosity analyzer with N_2 as the adsorption gas. NH_3-TPD was recorded in a Quantachrome automated chemisorption analyzer from room temperature to 850 °C with a ramp of 10 °C min^{-1}. The Si/Al of the zeolite was obtained by an inductively coupled plasma optical emission spectrometer (ICP-OES, IRIS Intrepid II XSP). NMR spectra were obtained on a Varian Infinityplus-400 spectrometer. Brønsted acid sites and Lewis acid sites were determined by pyridine adsorption. The samples were first dried, *in situ*, by heating to 723 K under vacuum, and then were cooled to 323 K. At this temperature, the samples

were exposed to pyridine vapor using an equilibration time of 30 min. After the physically adsorbed pyridine molecules were removed by outgassing at 423 K for 1 h, IR spectra were collected at 423 K with 4 cm^{-1} resolution using a Nicolet FTIR spectrometer.

2.3. Catalytic conversion of methanol to aromatics

Before the catalytic test, all the samples were modified with 2 wt% Zn by traditional incipient wetness impregnation using aqueous solutions of Zn $(NO_3)_2 \cdot 6H_2O$. Then the Zn-modified samples were dried overnight and calcinated in air at 823 K for 5 h.

The MTA reactions were performed at the conditions of 1 atm, 748 K and WHSV = 0.75 h^{-1} (under N_2 flow (10 mL min^{-1})) in a conventional fixed bed stainless steel reactor (13.0 mm i.d.) equipped with a thermocouple in the middle of the catalyst bed. 0.70 g of catalyst was placed in the fixed bed reactor. The flow rate of the pure methanol and N_2 was controlled using a dual micro-plunger pump and the mass flow controllers, respectively. The products (hydrocarbons) were analyzed using two flame ionization detectors (FIDs). The conversion of methanol and the selectivity of the different products were calculated (carbon base) by considering the oxygenates (methanol and dimethylether) as the unconverted reactant.

2.4. Analysis of partially deactivated catalysts

The partially deactivated catalysts after the catalytic tests were characterized by TGA-DSC, nitrogen adsorption, TEM and GC-MS to investigate the factors resulting in the superior catalytic performance of the nanosized ZSM-5. TGA-DSC was performed using a thermo-gravimetric analyzer (TGA/DSC-1) in the range 30–900 °C at a heating rate of 10 °C min^{-1} in air. The coke species formed on the deactivated catalysts after reactions were also characterized by gas chromatography-mass spectroscopy (GC-MS). The coke species were extracted by the following method developed by Guisnet[34] with a slight modification. To obtain the relative concentrations of the organics formed over different samples, the exactly same amount (20 mg) of the deactivated catalyst was always dissolved in 1 mL of 15% HF solution. Organic species were then extracted with 0.8 mL $C(CH_3)_2Cl_2$ and analyzed using GC-MS (MSD 5973, EI 70 eV) with a HP-5MS column (30 m, 0.25 mm i.d.), and the graphite carbon in the water phase was characterized by TEM experiments.

Furthermore, the location and the amount of coke in Zn/NZS-60 were analyzed as a function of the reaction time, using the previously reported methods.[35–37] The total amount of coke (external + internal) within the partially deactivated Zn/NZS-60 at different reaction times was obtained using TGA analysis. The amount of the internal coke was estimated from the decrease in the micropore volume (determined by the N_2 adsorption measurements) relative to the pristine sample, by assuming a coke density of 1.22 g cm^{-3}. The external coke was calculated by subtracting the internal coke content from the total coke content.

3. Results and discussion

3.1. Characterization of the fresh ZSM-5 samples

The preparation of N-ZSM-5 is also shown schematically in Fig. 1. The steam assisted conversion (SAC) method is a very efficient method for preparing zeolites.[38–41] In our route using the SAC method, a little amount of water necessary for crystallization is always kept separate from the precursor powder during the crystallization reactions. Obviously, after the crystallization process, the products are in the solid phase, free of alkali ions, which could be directly converted to the H-form nanosized ZSM-5 for acid catalytic applications only *via* calcination. In addition, the avoidance of solvents in the synthesis and the repeated wash processes for removing NaOH not only significantly reduces the waste production, but also significantly enhances its crystallization efficiency along with a high yield.

Fig. 2 shows the representative low and high magnification SEM images of the nanosized ZSM-5 prepared by our route. The SEM images clearly show that the N-ZSM-5 is composed of many spherical crystallites with uniform sizes of about 50 nm. To further confirm the particle sizes and the structure, the nanosized ZSM-5 were studied by transmission electron microscopy (TEM). The TEM images (Fig. 3a–c) reveal an abundant mesoporous network through the assembly of these uniform nanosized ZSM-5 crystals. Analysis with HR-TEM images in Fig. 3d–f elucidates that all the samples are completely crystalline, as the parallel lattice fringes can be clearly observed and are clearly spread throughout the entire crystals. Individual particles can be recognized with average sizes of about 50 nm. Obviously, the Si/Al of the ZSM-5 precursor hardly affects the size and morphology of the final products, which is different from the general pattern when using hydrothermal methods.[42] The absence of a sponge-like material in the SEM and TEM pictures indicates the absence of amorphous material. Since no silica and aluminium source are washed away in the entire synthetic route, the yield of these nanosized ZSM-5 is nearly 100%, in stark contrast to the low yields of nanoparticles usually obtained from the conventional hydrothermal route.[27,29,42,43]

The stacking of these nanosized crystals produces the substantial mesoporosity, leading to a different pore structure from the conventional ZSM-5 (Fig. S2†). Nitrogen adsorption/desorption isotherms and BJH pore size distribution are shown in Fig. 4. The CZS-30 shows a typical type-I isotherm

Fig. 1 Schematic diagram of centrifugation-free synthetic procedures for nanosized ZSM-5 with tunable Si/Al molar ratios.

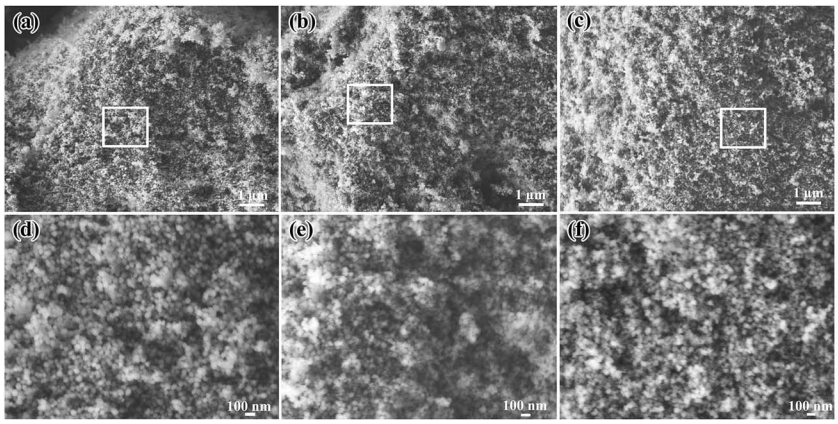

Fig. 2 SEM images of (a) NZS-30, (b) NZS-60, and (c) NZS-90, and the high-magnification SEM images of (d) NZS-30, (e) NZS-60, and (f) NZS-90, which are taken from the part surrounded with a white frame in (a), (b), and (c).

corresponding to the solely microporous structure. However, all isotherms of the nanosized H-ZSM-5 exhibit a typical adsorption curve of type I plus type IV with an apparent enhanced uptake and an obvious hysteresis loop in the P/P_o range of 0.8 to 1, indicating its remarkable micro-/mesoporous structure.[24,44,45] Correspondingly, pore size analysis by the BJH method using the adsorption branch of the isotherm (Fig. 4b) shows that all the nanosized H-ZSM-5 possess a broad pore distribution with a mean pore size of about 20 nm. As a result, the nanosized H-ZSM-5 have a much higher BET area and a larger mesopore volume than the CZS-30. As summarized in Table 1, the BET surface area increases from 388 $m^2\ g^{-1}$ for the CZS-30 up to 441.5–484.0 $m^2\ g^{-1}$ for nanosized ZSM-5. The total pore volume increases from 0.19 $cm^3\ g^{-1}$ to 0.72–0.76 $cm^3\ g^{-1}$ and the mesopore volume increases from 0.04 $cm^3\ g^{-1}$ to more than 0.58–0.62 $cm^3\ g^{-1}$. It is also worth noting that the textural properties do not noticeably change while increasing the Si/Al of the nanosized H-ZSM-5.

The XRD patterns of all the samples (Fig. 5a) show five well-resolved peaks at 7.98°, 8.82°, 23.18°, 24.02° and 24.46°, which are in good agreement with the highly crystalline MFI-structured ZSM-5 without any impurities or amorphous phase.[30,46] The XRD line widths of all the nanosized H-ZSM-5 are much broader than those for CZS-30 due to their smaller crystal size.[47] Fig. 5b shows the UV Raman spectra of the samples excited at 325 nm. All the samples show the characteristic bands of the MFI structure with a wide band at 380 cm^{-1} (Fig. 5b), which is associated with the framework symmetric stretching vibration of a five-membered building unit in the ZSM-5

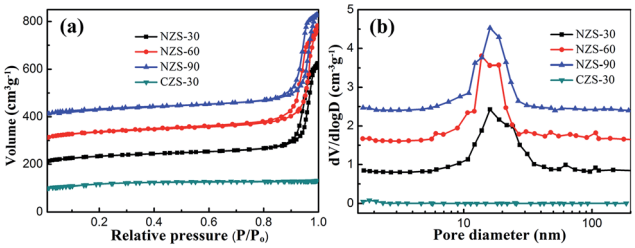

Fig. 4 (a) Nitrogen adsorption/desorption isotherms and (b) BJH pore size distribution curves calculated from the adsorption branch of the isotherm (inset) for NZS-30, NZS-60, NZS-90, and CZS-30.

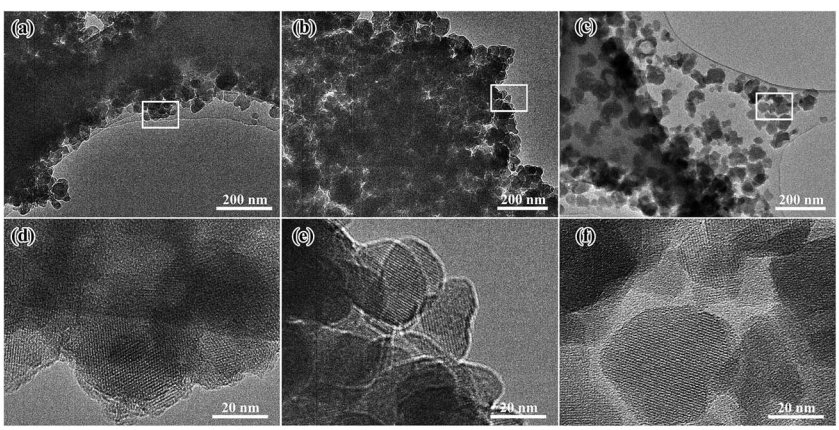

Fig. 3 Low-magnification TEM images of (a) NZS-30, (b) NZS-60, and (c) NZS-90, and the high-magnification TEM images of (d) NZS-30, (e) NZS-60, and (f) NZS-90, which are taken from the part surrounded with a white frame in (a), (b), and (c).

Table 1 Textural properties and compositions of various samples

Sample name	Si/Al_{th} atomic ratio[a] (mol mol^{-1})	Si/Al_{ICP} atomic ratio[b] (mol mol^{-1})	BET surface area (m^2 g^{-1})	Mesopore surface area[c] (cm^3 g^{-1})	Total pore volume (cm^3 g^{-1})	Micropore volume[c] (cm^3 g^{-1})	Mesopore volume[d] (cm^3 g^{-1})
CZS-30	30	24.1	388.2	33.1	0.19	0.15	0.04
NZS-30	30	28.6	484.0	118.6	0.73	0.15	0.58
NZS-60	60	56.2	441.5	100.4	0.72	0.14	0.58
NZS-90	90	84.4	446.7	107.7	0.76	0.14	0.62

[a] The theoretical Si/Al based on the molar composition of the initial gel. [b] Measured by ICP-OES. [c] *t*-plot method. [d] $V_{meso} = V_{tot} - V_{micro}$.

zeolites.[32,48,49] Generally, the catalytically active acid sites of ZSM-5 are always correlated to the presence of intra-framework aluminium atoms. Thus, successful incorporation of aluminium atoms into the silica framework of nanosized ZSM-5 with a wide Si/Al_{th} is verified by ^{27}Al MAS NMR spectroscopy. As shown in Fig. 5c, the ^{27}Al MAS-NMR spectra of all the samples show only one sharp aluminium peak at 52 ppm, indicating that all the aluminium atoms are incorporated into the ZSM-5 framework with a tetrahedral coordination environment.[50] In addition, the ^{29}Si MAS NMR spectra of all the samples (Fig. S3†) show similar features with a sharp peak at −112 ppm and a small peak at −105 ppm. The sharp peak can be attributed to the Si(0Al) contribution, and the small peak to the Si(1Al) contribution,[51] which further confirm the presence of framework aluminium in the nanosized ZSM-5. Thus, nanosized ZSM-5 with a wide range of Si/Al can be prepared directly by this facile direct synthesis route.

Furthermore, the different textural properties brought about by the crystal sizes might induce remarkable changes of surface properties, which play a crucial role in the catalytic performance of the zeolite-based catalysts. The infrared spectra of the dehydrated form of CZS-30 (Fig. 5d) show no obvious peaks because of the broad background peak. In sharp contrast, the infrared spectra of three nanosized ZSM-5 in the region of the OH stretching vibrations show a major band at 3745 cm^{-1}, attributed to silanol groups, which is in agreement with its decreased crystal sizes and increased external surface area. It is reported that this type of Si-related defective site is very effective for increasing the yields of aromatics and paraffins for the MTH reaction.[52] Besides, additional spectral components of lower intensity are found over nanosized ZSM-5, which could be attributed to: (1) perturbed silanols mainly located inside the zeolite crystals (3727 cm^{-1}), (2) Al(OH)Si groups corresponding to strongly acidic Brønsted sites (3612 cm^{-1}), and (3) a broad

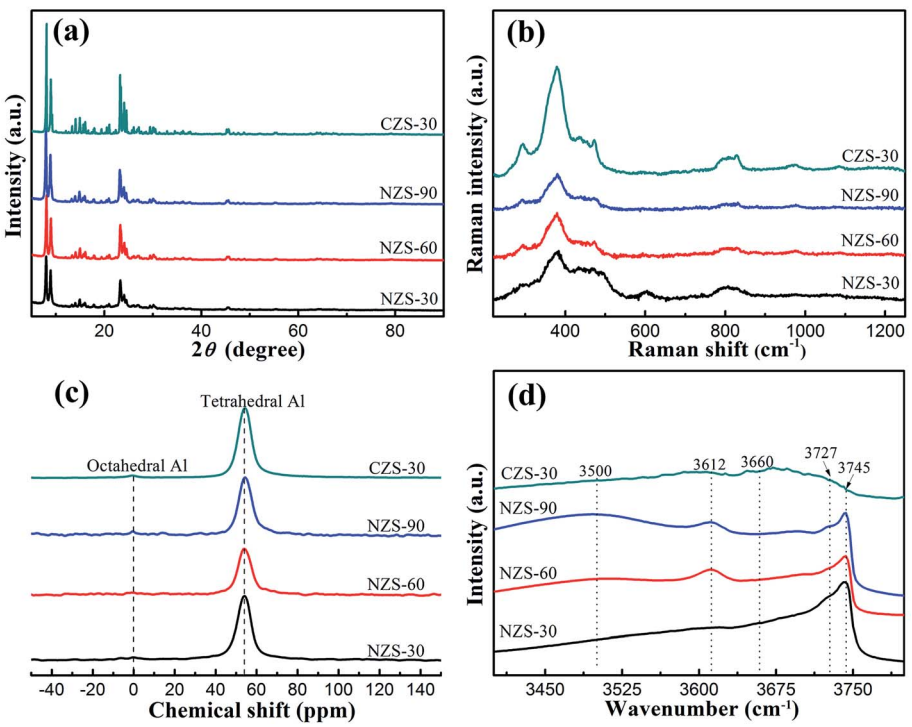

Fig. 5 (a) XRD patterns, (b) UV-Raman spectra, and (c) ^{27}Al-NMR spectra of the NZS-30, NZS-60, NZS-90, and CZS-30. (d) FT-IR spectra of the dehydrated NZS-30, NZS-60, NZS-90, and CZS-30.

band corresponding to silanols interacting through hydrogen bonding (3500 cm^{-1}). As for NZS-60 and NZS-90, the intensity of the bands at 3745 cm^{-1} and 3500 cm^{-1} are stronger than NZS-30, suggesting that the Si/Al of nanosized ZSM-5 could influence its surface characteristics significantly. There are hardly any peaks at about 3660 cm^{-1} ascribed to OH groups bound to extra-framework and/or perturbed framework Al atoms,[52,53] indicating the successful incorporation of all the aluminium atoms into the silica framework of the samples.

In order to certify the feasibility of our synthesis route, we compared the acidic properties of pristine nanosized ZSM-5 and the samples after 3 times of ion-exchange. As shown in Fig. 6, minor differences are observed in both the TPD curves (Fig. 6a) and in the pyridine-absorbed FTIR spectra (Fig. 6b) between the three couples of nanosized ZSM-5, indicating that an energy-intensive centrifugal separation and ion-exchange process are indeed unnecessary in our route. In addition, Fig. 6a shows that the acid strength is declined sharply with the increase in Si/Al for the nanosized H-ZSM-5, and that the acidity of NZS-30 is also comparable with CZS-30 because of their similar Si/Al_{ICP} (Table 1). It is also noteworthy that the amount of L acid reduces rapidly with the increase in Si/Al of the nanosized H-ZSM-5 (Fig. 6b). Moreover, the intensity of the hydrogen-bonded PyH^+ peak over nanosized ZSM-5 is much stronger than in CZS-30, due to the enhanced adsorption capacity caused by its large mesopore volume.[54]

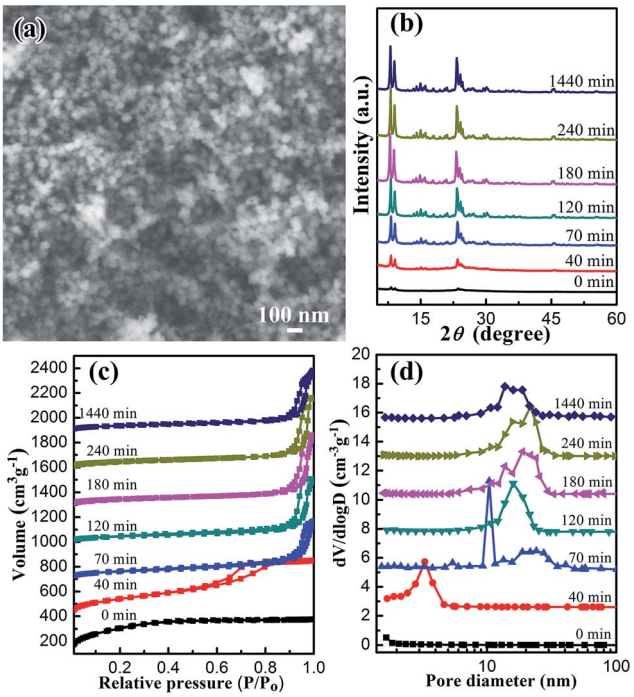

Fig. 7 Investigation into the crystallization process of NZS-60. (a) SEM image of the product crystallized at 180 °C for 180 min, (b) XRD patterns, (c) Nitrogen adsorption/desorption isotherms, and (d) BJH pore size distribution calculated from the adsorption branch of the isotherm for the samples crystallized at various crystallization times.

3.2. Evolution of the nanosized ZSM-5 with crystallization time

To study the crystallization mechanism of NZS-60, a kinetic run was carried out by varying the synthesis time from 0 h to 24 h at 180 °C. Fig. 7b shows the XRD patterns of the samples at different reaction times. Before stream-assisted crystallization, the sample exhibited an extremely faint XRD pattern of a MFI structure. With the steam-assisted conversion at 180 °C, the intensity of the characteristic MFI-structured peaks increased rapidly and drew the maximum as crystallization proceeded up to 3 h, which indicated that the amorphous structure of the starting powder could translate into a pure ZSM-5 phase just within 3 h (Fig. 7a). Obviously, the presence of seeds plays an important role in shortening the nucleation stage, which is the most time consuming step in the crystallization of ZSM-5.[49] Interestingly, further increasing the crystallization time leads to the slight reduction of crystallinity, possibly due to the destructive effect of the template on the framework of the product. It is well reported that the TPAOH template plays the role of a scaffold forming a mesostructure during the crystallization process.[55] This is confirmed by the N_2 adsorption isotherm and the corresponding pore size distribution. As shown in Fig. 7c, the isotherm of the sample with 0 h crystallization has a near linear uptake over the P/P_o range from 0 to 0.4, which corresponds to micropores or small mesopores

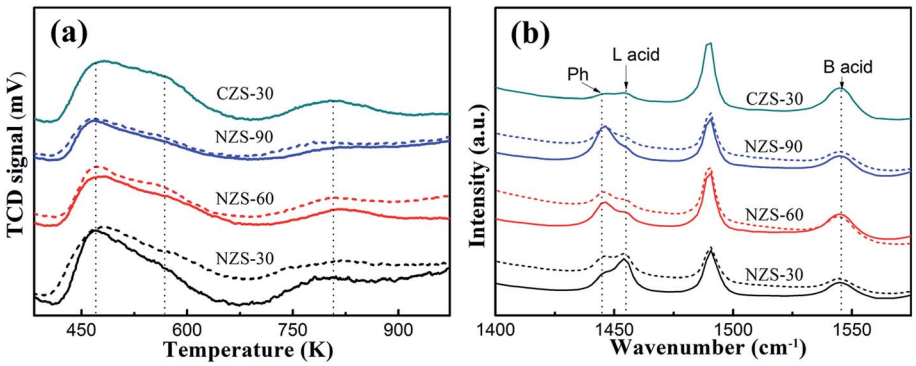

Fig. 6 (a) NH_3-TPD adsorption spectra of the NZS-30, NZS-60, NZS-90, and CZS-30. (b) FTIR spectra of the dehydrated NZS-30, NZS-60, NZS-90, and CZS-30.

Table 2 Textural properties and crystallinity of the NZS-60 crystallized at various times

Crystallization time (min)	Crystallinity[a] (%)	BET surface area ($m^2\ g^{-1}$)	Mesopore surface area[b] ($cm^3\ g^{-1}$)	Total pore volume ($cm^3\ g^{-1}$)	Micropore volume[b] ($cm^3\ g^{-1}$)	Mesopore volume[c] ($cm^3\ g^{-1}$)
0	0.04	1081.5	—[d]	0.58	—[d]	—[d]
40	19.37	854.0	547.4	0.84	0.14	0.70
70	54.46	593.9	189.3	0.88	0.16	0.72
120	75.57	519.9	137.0	0.93	0.17	0.76
180	100.00	472.8	119.4	0.86	0.15	0.71
240	99.87	466.4	115.6	0.77	0.15	0.62
1440	95.10	441.5	100.4	0.72	0.14	0.58

[a] Calculated *via* XRD result by assuming the maximum crystallinity of the product after 180 min of crystallization time is 100%. [b] *t*-plot method. [c] $V_{meso} = V_{tot} - V_{micro}$. [d] *t*-plot is not applicable because of the continuous distribution of pore sizes around 3 nm.

below 3 nm. Upon increasing the crystallization time from 0 h to 180 min, the uptakes of the isotherms move toward high P/P_o. Correspondingly, the average pore size increases from less than 3 nm in the starting dry gel to about 11 nm in the sample at 180 min crystallization time. A longer crystallization treatment has little effect on the mesoporous structure, since no obvious changes can be observed from the pore size distribution curves. Table 2 summarizes the textural properties and crystallinity of the samples at various crystallization times. The external surface area decreases with crystallization time, but remains very high, even after reaching 100% crystallization. However, both the total pore volume and the mesopore volume increase within 120 min crystallization time, and finally achieve stability, indicating the high efficiency of our route for obtaining meso/micropore zeolites (Table 2).

3.3. Effects of gel composition and aging conditions

In our preliminary experiments, we discovered that the crystal size of the products was sensitive to the concentrations of NH_4^+. Therefore, at an aging temperature of 90 °C for 72 h and a constant Si/Al_{th} of 60, the influence of NH_4^+/SiO_2 was investigated, and the SEM images of products prepared with different NH_4NO_3/SiO_2 are shown in Fig. 8. When there is no NH_4NO_3 added into the synthesis mixture, the size distribution of the product is broad and most of the ZSM-5 crystals are greater than 100 nm. Products with a uniform diameter of about 50 nm could be obtained with a NH_4/SiO_2 ratio of 0.017–0.034 (Fig. 8b and c). This can be explained by the fact that aluminium incorporation is achieved more easily when the smaller NH_4^+ are available as charge compensators, compared with the situation when only the larger TPA^+ are present. Further increasing the NH_4^+ to 0.067, a sample with a diameter of about 300 nm and a smaller BET surface area was obtained. The increased particle size and the reduced crystallinity of the ZSM-5 crystals obtained in this run were probably due to the excessively decreased alkalinity, caused by the hydrolysis of plentiful NH_4^+.

In addition, our synthesis route includes the "pre-aging process" before stream-assisted crystallization, which is considered to produce abundant ZSM-5 nuclei (Fig. S1†),[56] leading to the formation of small ZSM-5. Hence, the effect of the pre-aging time on the crystal size of the product was also investigated, but with other conditions remaining unchanged. Fig. 9 shows the SEM images of the products synthesized with the pre-aging temperature of 90 °C for different times, which indicate that the crystal size is decreased with the increase in pre-aging time. The average crystal sizes of the products at pre-aging times of 0, 24, and 72 h were found to be about 160 nm, 100 nm, and 50 nm, respectively. A further extension of the aging time after 72 h had little effect on the crystalline phases and crystal size, since no obvious changes could be observed from the SEM image.

3.4. Catalytic performances of the nanosized ZSM-5 with different Si/Al

The methanol to aromatics reaction (MTA) is an important process for the non-oil route to aromatics.[10–12,57] It is respected that the meso/macroporous structure and the short diffusion length of nanosized ZSM-5 are favorable for the MTA reaction with high stability. Therefore, the catalytic performances over 2% Zn-modified nanosized (denoted as Zn/NZS-30, Zn/NZS-60, and Zn/NZS-90) and 2% Zn-modified conventional ZSM-5

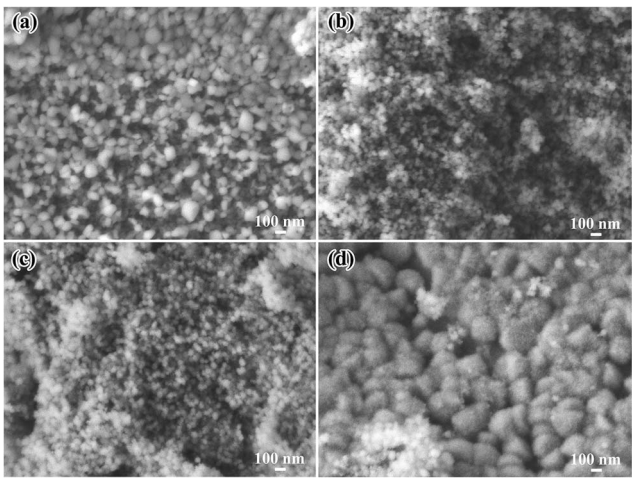

Fig. 8 SEM images of the NZS-60 prepared with an NH_4NO_3/SiO_2 molar ratio of (a) 0, (b) 0.017, (c) 0.034, and (d) 0.067, indicating that a trace amount of NH_4NO_3 addition to the precursor gel markedly reduces the particle sizes of the NZS-60.

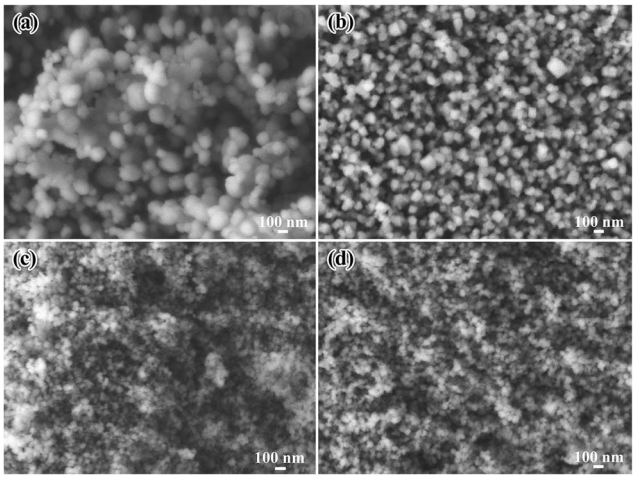

Fig. 9 SEM images of the NZS-60 prepared with an aging time of (a) 0 h, (b) 36 h, (c) 72 h, and (d) 144 h, indicating that the particle size of NZS-60 is decreased with an increase in the pre-aging time.

(denoted as Zn/CZS-30, Zn/CZS-60, and Zn/CZS-90) in the MTA reaction were compared in a fixed bed stainless steel reactor. Fig. 10 shows an overview of the activities and stabilities of the three groups between nanosized and conventional ZSM-5 described in this contribution. It is worth noting that the comparison of catalysts performance was performed under the same Si/Al_{th} ratios, because the catalytic properties are more likely to change by Al content. Under such a strict operation condition, all the catalysts showed almost the similar high initial methanol conversions of above 95% (Table 3). However, as the reaction proceeded, the activities of Zn/CZS-30, Zn/CZS-60, and Zn/CZS-90 all declined gradually within just a few hours. In sharp contrast, all the nanosized ZSM-5 showed a more superior catalytic stability and a higher total aromatics selectivity than the corresponding conventional Zn/ZSM-5 with the same Si/Al_{th}. It is noted that the Si/Al_{th} ratios also have a remarkable effect on the catalytic performance of nanosized Zn/ZSM-5 catalysts. Among these catalysts, the Zn/NZS-60 with $Si/Al_{th} = 60$ gives the slowest deactivation with a stable total aromatics selectivity and long catalytic lifetime (defined as the time at which the catalytic conversion decreases by 50%, which is denoted as $t_{1/2}$) of more than 75 h, which is almost 25-fold that of Zn/CZS-60 ($t_{1/2} \approx 3$ h). In addition, the detailed initial product selectivity is also given in Tables S2 and S3.† Notably, the most stable Zn/NZS-60 shows a high total aromatics selectivity of 68%, with an absolute selectivity of 16% higher than the CZS-60 (52%). More importantly, the selectivity of 1,2,4-trimethylbenzene over this catalyst can be up to 44% for all products and 64% for aromatics products (Table 4). Compared with the previously reported results in the process of MTA,[13] the high selectivity of 1,2,4-trimethylbenzene over nanosized Zn/ZSM-5 could significantly reduce the cost and energy consumption of the subsequent separation and purification process to obtain high purity 1,2,4-trimethylbenzene. Since the acid strength, acid amount, Si/Al_{ICP} ratio, and micropore volume are all similar for Zn/NZS-60 and Zn/CZS-60 (Fig. 6 and Table 1), the superior catalytic stability and higher 1,2,4-trimethylbenzene selectivity over the former can be directly attributed to the unique mesoporous structure and short diffusion length of the nanosized ZSM-5. It is well documented that the catalyst deactivation of ZSM-5 is mainly caused by coke formation on the micropore mouths and in the micropores, which are produced *via* secondary reactions.[37,58] Hence, micropore blockage could occur very slowly over the nanosized ZSM-5 because of its unique mesoporous structure and the abundant pore mouths at the surface of the nanosized ZSM-5, both of which not only favor the coke precursor diffusion, but also sharply increase the evacuation of aromatics and make the isomerization reaction of trimethylbenzene dynamically balanced, leading to the high selectivity of 1,2,4-trimethylbenzene, which is the most thermodynamically stable product when the isomerization reaction of trimethylbenzene reaches thermodynamic equilibrium. Due to the enlarged external surface area and short diffusion path lengths, it is feasible that the thermodynamically stable 1,2,4-trimethylbenzene formed inside the micropores could readily migrate to the external surface. In the case of solely microporous Zn/CZS-60, the diffusion of this bulk product from the micropores to the external surface would be relatively slow, leading to a lower aromatics selectivity and shorter lifetime in the MTA process.

In order to verify this point, we conducted a series of characterization tests over the spent Zn/NZS-60 and Zn/CZS-60, including TG/DSC, GC-MS, and TEM. The TG/DTA profiles are shown in Fig. 11. It is obvious that the total weight loss over the spent Zn/NZS-60 is obviously much higher than that over

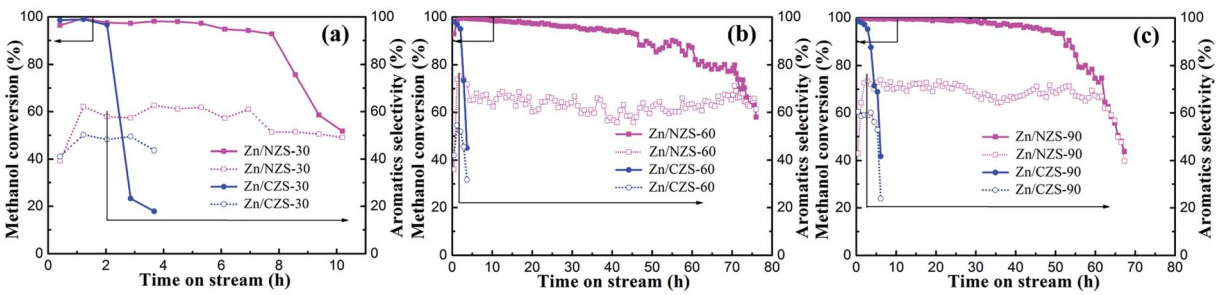

Fig. 10 Methanol conversions and overall aromatics selectivity with various Zn/ZSM-5 samples as a function of time-on-stream (reaction temperature: 475 °C; reaction pressure: atmospheric pressure, WHSV: 0.75 h^{-1}).

Table 3 Methanol conversion and product selectivity of MTA reactions over various catalysts used in the present study measured after the reactions were stable

Catalysts[a]	Conversion of methanol (%)	Selectivity, (%)						Total aromatics (%)
		C_1–C_5 alkanes	C_2–C_5 olefins	C_6 ben.	C_7 ben.	C_8 ben.	C_{9+} ben.	
Zn/CZS-30	99.03	20.83	28.95	1.76	11.19	36.09	1.16	50.22
Zn/CZS-60	96.80	16.77	31.23	0.64	5.29	34.57	11.49	51.99
Zn/CZS-90	95.54	16.02	27.43	0.81	7.19	31.88	16.65	56.54
Zn/NZS-30	99.47	15.06	22.80	0.48	3.71	25.88	32.07	62.15
Zn/NZS-60	99.37	24.36	7.69	0.32	2.07	14.60	50.95	67.94
Zn/NZS-90	99.41	18.12	11.32	0.50	3.20	14.62	52.21	70.55

[a] The sampling time (Zn/CZS-30, Zn/CZS-60, Zn/CZS-90: 1.2 h, Zn/NZS-60: 3.6 h, and Zn/NZS-90: 10.2 h).

conventional ZSM-5, indicating its much higher capacity for holding coke. However, as the reaction time of Zn/NZS-60 is much longer than the corresponding Zn/CZS-60, the spent Zn/NZS-60 has a slow coke formation rate of 3.78 mg g_{cat}^{-1} h^{-1}, much lower than that of 26.33 mg g_{cat}^{-1} h^{-1} for spent Zn/CZS-60. As shown in Fig. 11b, the DTA profiles of the spent Zn/CZS-60 has a broad exothermic peak, implying that the coke in this catalyst is composed of various carbon species deposited on active sites. However, there is almost only one sharp exothermic peak around 480 °C for NZS-60, indicating that the carbon species formed over this catalyst is mainly a relatively single coke species, which is also confirmed by the GC-MS analysis of the retained organic species in spent catalysts by 15% HF dissolution and extraction. As shown in Fig. 12a and b, only a tiny amount of liberating heavy hydrocarbons could be found in the extract phase of Zn/NZS-60, and the main phase of deposits over this sample was graphite carbon, which could not be extracted by CH_2Cl_2 (Fig. 12a). However, significant amounts of polyaromatic hydrocarbon are found over conventional ZSM-5, which could occlude the pore channel and lead to the quick deactivation of the catalysts (Fig. 12b).

Furthermore, in order to understand how the particle size of ZSM-5 is related to the catalytic performance, the location and the amount of coke in Zn/NZS-60 were analyzed as a function of the reaction time using the characterization method described in Section 2.4. As the results in Fig. 12c

Table 4 The distribution of trimethylbenzene selectivity over various catalysts used in the present study measured after the reactions were stable

Catalysts[a]	Selectivity in products, (%)			Selectivity in aromatics, (%)		
	1,3,5-Tri-ben	1,2,4-Tri-ben	1,2,3-Tri-ben	1,3,5-Tri-ben	1,2,4-Tri-ben	1,2,3-Tri-ben
Zn/CZS-30	—	1.16	—	—	2.31	—
Zn/CZS-60	—	10.92	—	—	21.00	—
Zn/CZS-90	0.53	15.52	0.58	0.94	27.45	1.03
Zn/NZS-30	2.38	27.66	2.02	3.83	44.51	3.25
Zn/NZS-60	3.90	44.12	2.92	5.74	64.94	4.30
Zn/NZS-90	4.53	44.40	3.57	6.42	62.93	5.06

[a] The sampling time (Zn/CZS-30, Zn/CZS-60, Zn/CZS-90: 1.2 h, Zn/NZS-60: 3.6 h, and Zn/NZS-90: 10.2 h).

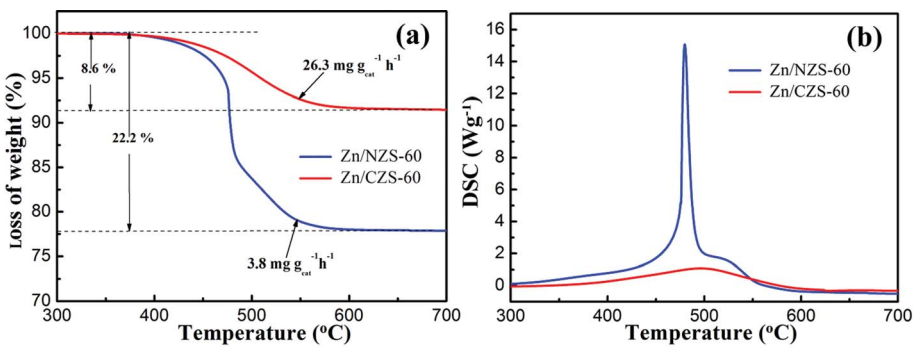

Fig. 11 (a) TG and (b) DSC profiles of the spent Zn/CZS-60 and Zn/NZS-60. Oxidation gas: 20% O_2/N_2, heating rate 10 °C min^{-1}.

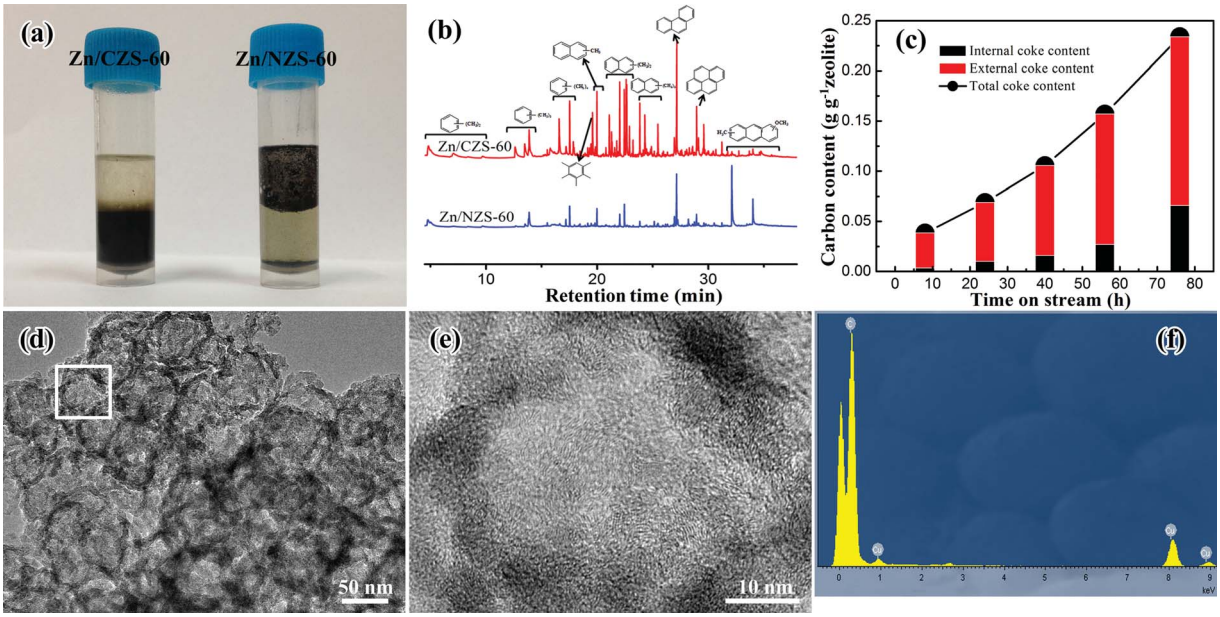

Fig. 12 (a) Photographs of the spent catalysts after being dissolved in 15% HF and extracted by CCl_4. (b) GC-MS chromatograms of the organic species in spent catalysts extracted by CH_2Cl_2. (c) Coke formation over Zn/NZS-60 with various time-on-stream during the MTA reaction. (d) and (e) TEM images of the graphite carbon depositing on the outer surface of Zn/NZS-60 after the inner Zn/NZS-60 is dissolved by 15% HF solution. (f) The corresponding EDX spectrum of the graphite carbon.

show, the coke in Zn/NZS-60 is preferentially deposited at the stacking pores of nanosized ZSM-5 prior to the generation inside the straight and sinusoidal channels with a much slower coking rate than Zn/CZS-60. The coke in the stacking pores is not completely blocked, and the reactants and products could still move to the active sites and escape from the micropores. The TEM images and the corresponding EDX analysis of the graphite carbon also verify the above results. As shown in Fig. 12d and e, the graphite carbon, as deposited on the outer surface of Zn/NZS-60, forms hollow carbon nanospheres after the inner Zn/NZS-60 is dissolved by 15% HF solution. However, 89% of the coke is formed inside the micropore for the Zn/CZS-60 with solely micropores, which is the main cause of the sudden drop in catalytic activity. Therefore, we, for the first time, validate directly that the coke over nanosized ZSM-5 is preferentially deposited on the outside surface prior to the intracrystalline micropores. Above all, compared with conventional ZSM-5, the nanosized ZSM-5 has the following obvious advantages when used in the MTA reaction: (1) short diffusion length, which could enhance the diffusibility of reactants and products and prevent the deposition of polyaromatic hydrocarbons in the microspores; (2) substantial mesoporosity, which endows the nanosized ZSM-5 with a much higher capacity for holding coke than the conventional one; (3) high external surface, which sharply increases the reaction efficiency of bulky intermediate products on the surface of the catalyst, leading to a high selectivity of 1,2,4-trimethylbenzene; (4) abundant surface groups (*e.g.*, silanol groups, perturbed silanols, and Al(OH)Si groups) could provide more active sites for the MTA reaction.

4. Conclusions

The present work reports a centrifugation-free synthesis route for hierarchical nanosized ZSM-5 with 100% yield by steam-assisted conversion using a solid alkalis-free powder as the ZSM-5 precursor. The obtained nanosized ZSM-5 possesses excellent properties, such as ultrafine uniform size, robust thermal stability, high surface area, high total pore volumes, tunable Si/Al molar ratio, and high crystallinity, and shows excellent catalytic performance when used in the catalytic conversion of methanol to aromatics. The Zn/NZS-60 shows an almost 25-fold catalyst lifetime and up to 16% higher total aromatics selectivity compared with conventional microsized Zn/CZS-60. More importantly, the selectivity of 1,2,4-trimethylbenzene over this catalyst can be up to 44% for all products and 64% for aromatics products. Analysis of the partially deactivated catalysts revealed that the superior catalytic stability and higher 1,2,4-trimethylbenzene selectivity over the nanosized Zn/ZSM-5 could be directly attributed to its small crystal size and mesoporous structure, which prevent the deposition of polyaromatic hydrocarbon in the micropores, but also sharply increase the reaction efficiency of the bulky molecule. The nanosized ZSM-5 prepared by this route shows immense potential for large scale industrial applications for the MTA process with a high selectivity of 1,2,4-trimethylbenzene.

Conflict of interest

The authors declare no competing financial interest.

Acknowledgements

This work was supported by NSFC program of 21376135 and NSFC key program of 51236004.

References

1 T. R. Carlson, Y. T. Cheng, J. Jae and G. W. Huber, *Energy Environ. Sci.*, 2011, **4**, 145.
2 B. Valle, A. G. Gayubo, A. T. Aguayo, M. Olazar and J. Bilbao, *Energy Fuels*, 2010, **24**, 2060.
3 T. R. Carlson, J. Jae, Y.-C. Lin, G. A. Tompsett and G. W. Huber, *J. Catal.*, 2010, **270**, 110.
4 X. Guo, G. Fang, G. Li, H. Ma, H. Fan, L. Yu, C. Ma, X. Wu, D. Deng and M. Wei, *Science*, 2014, **344**, 616.
5 L. Yu, S. Huang, S. Zhang, Z. Liu, W. Xin, S. Xie and L. Xu, *ACS Catal.*, 2012, **2**, 1203.
6 Y. T. Cheng and G. W. Huber, *ACS Catal.*, 2011, **1**, 611.
7 Y. T. Cheng, Z. Wang, C. J. Gilbert, W. Fan and G. W. Huber, *Angew. Chem., Int. Ed.*, 2012, **51**, 11097.
8 T. F. Degnan Jr, *Top. Catal.*, 2000, **13**, 349.
9 C. Marcilly, *J. Catal.*, 2003, **216**, 47.
10 K. Shen, W. Qian, N. Wang, J. Zhang and F. Wei, *J. Mater. Chem. A*, 2013, **1**, 3272.
11 R. Barthos, T. Bánsági, T. Süli Zakar and F. Solymosi, *J. Catal.*, 2007, **247**, 368.
12 Y. Ni, A. Sun, X. Wu, G. Hai, J. Hu, T. Li and G. Li, *Microporous Mesoporous Mater.*, 2011, **143**, 435.
13 C. S. Cundy and P. A. Cox, *Chem. Rev.*, 2003, **103**, 663.
14 A. Corma, *Chem. Rev.*, 1997, **97**, 2373.
15 F. Pan, X. Lu, Y. Wang, S. Chen, T. Wang and Y. Yan, *Microporous Mesoporous Mater.*, 2014, **184**, 134.
16 D. Van Vu, M. Miyamoto, N. Nishiyama, Y. Egashira and K. Ueyama, *J. Catal.*, 2006, **243**, 389.
17 M. B. Roeffaers, R. Ameloot, M. Baruah, H. Uji-i, M. Bulut, G. De Cremer, U. Müller, P. A. Jacobs, J. Hofkens and B. F. Sels, *J. Am. Chem. Soc.*, 2008, **130**, 5763.
18 V. Valtchev, E. Balanzat, V. Mavrodinova, I. Diaz, J. El Fallah and J.-M. Goupil, *J. Am. Chem. Soc.*, 2011, **133**, 18950.
19 H. Jin, M. B. Ansari and S.-E. Park, *Chem. Commun.*, 2011, **47**, 7482.
20 S. I. Cho, S. D. Choi, J. H. Kim and G. J. Kim, *Adv. Funct. Mater.*, 2004, **14**, 49.
21 C. H. Jacobsen, *Chem. Commun.*, 1999, 673.
22 I. Schmidt, C. Madsen and C. J. Jacobsen, *Inorg. Chem.*, 2000, **39**, 2279.
23 P.-S. Lee, X. Zhang, J. A. Stoeger, A. Malek, W. Fan, S. Kumar, W. C. Yoo, S. Al Hashimi, R. L. Penn and A. Stein, *J. Am. Chem. Soc.*, 2010, **133**, 493.
24 H. Chen, J. Wydra, X. Zhang, P.-S. Lee, Z. Wang, W. Fan and M. Tsapatsis, *J. Am. Chem. Soc.*, 2011, **133**, 12390.
25 W. C. Yoo, S. Kumar, R. L. Penn, M. Tsapatsis and A. Stein, *J. Am. Chem. Soc.*, 2009, **131**, 12377.
26 W. Fan, M. A. Snyder, S. Kumar, P.-S. Lee, W. C. Yoo, A. V. McCormick, R. L. Penn, A. Stein and M. Tsapatsis, *Nat. Mater.*, 2008, **7**, 984.
27 R. Van Grieken, J. Sotelo, J. Menendez and J. Melero, *Microporous Mesoporous Mater.*, 2000, **39**, 135.
28 S. Lee, C. S. Carr and D. F. Shantz, *Langmuir*, 2005, **21**, 12031.
29 W. Song, V. Grassian and S. Larsen, *Chem. Commun.*, 2005, 2951.
30 Y.-Q. Deng, S.-F. Yin and C.-T. Au, *Ind. Eng. Chem. Res.*, 2012, **51**, 9492.
31 J. Aguado, D. Serrano and J. Rodriguez, *Microporous Mesoporous Mater.*, 2004, **75**, 41.
32 L. Ren, Q. Wu, C. Yang, L. Zhu, C. Li, P. Zhang, H. Zhang, X. Meng and F.-S. Xiao, *J. Am. Chem. Soc.*, 2012, **134**, 15173.
33 J. C. Groen, T. Bach, U. Ziese, A. M. Paulaime-van Donk, K. P. de Jong, J. A. Moulijn and J. Pérez-Ramírez, *J. Am. Chem. Soc.*, 2005, **127**, 10792.
34 M. Guisnet and P. Magnoux, *Appl. Catal.*, 1989, **54**, 1.
35 D. Bibby, N. Milestone, J. Patterson and L. Aldridge, *J. Catal.*, 1986, **97**, 493.
36 F. L. Bleken, K. Barbera, F. Bonino, U. Olsbye, K. P. Lillerud, S. Bordiga, P. Beato, T. V. Janssens and S. Svelle, *J. Catal.*, 2013, **307**, 62.
37 M. Choi, K. Na, J. Kim, Y. Sakamoto, O. Terasaki and R. Ryoo, *Nature*, 2009, **461**, 246.
38 S. P. Naik, A. S. Chiang and R. Thompson, *J. Phys. Chem. B*, 2003, **107**, 7006.
39 J. Yao, H. Wang, S. P. Ringer, K.-Y. Chan, L. Zhang and N. Xu, *Microporous Mesoporous Mater.*, 2005, **85**, 267.
40 K. Zhu, J. Sun, J. Liu, L. Wang, H. Wan, J. Hu, Y. Wang, C. H. Peden and Z. Nie, *ACS Catal.*, 2011, **1**, 682.
41 N. Ren, B. Subotić, J. Bronić, Y. Tang, M. Dutour Sikirić, T. Mišić, V. Svetličić, S. Bosnar and T. Antonić Jelić, *Chem. Mater.*, 2012, **24**, 1726.
42 V. B. Mortola, A. P. Ferreira, J. M. Fedeyko, C. Downing, J. M. Bueno, M. C. Kung and H. H. Kung, *J. Mater. Chem.*, 2010, **20**, 7517.
43 S. C. Larsen, *J. Phys. Chem. C*, 2007, **111**, 18464.
44 X. Liu, B. Tian, C. Yu, F. Gao, S. Xie, B. Tu, R. Che, L. M. Peng and D. Zhao, *Angew. Chem., Int. Ed.*, 2002, **41**, 3876.
45 M. Imperor-Clerc, P. Davidson and A. Davidson, *J. Am. Chem. Soc.*, 2000, **122**, 11925.
46 F. Liu, T. Willhammar, L. Wang, L. Zhu, Q. Sun, X. Meng, W. Carrillo-Cabrera, X. Zou and F.-S. Xiao, *J. Am. Chem. Soc.*, 2012, **134**, 4557.
47 J. Kim, M. Choi and R. Ryoo, *J. Catal.*, 2010, **269**, 219.
48 Y. Yu, G. Xiong, C. Li and F.-S. Xiao, *J. Catal.*, 2000, **194**, 487.
49 K. Shen, W. Qian, N. Wang, C. Su and F. Wei, *J. Am. Chem. Soc.*, 2013, **135**, 15322.
50 T.-O. Do, A. Nossov, M.-A. Springuel-Huet, C. Schneider, J. L. Bretherton, C. A. Fyfe and S. Kaliaguine, *J. Am. Chem. Soc.*, 2004, **126**, 14324.
51 C. Fyfe, G. Gobbi, G. Kennedy, J. Graham, R. Ozubko, W. Murphy, A. Bothner-By, J. Dadok and A. Chesnick, *Zeolites*, 1985, **5**, 179.
52 P. Sazama, B. Wichterlova, J. Dedecek, Z. Tvaruzkova, Z. Musilova, L. Palumbo, S. Sklenak and O. Gonsiorova, *Microporous Mesoporous Mater.*, 2011, **143**, 87.
53 S. Zheng, H. R. Heydenrych, A. Jentys and J. A. Lercher, *J. Phys. Chem. B*, 2002, **106**, 9552.

54 W. Song, R. Justice, C. Jones, V. Grassian and S. Larsen, *Langmuir*, 2004, **20**, 8301.
55 J. Wang, J. C. Groen, W. Yue, W. Zhou and M.-O. Coppens, *Chem. Commun.*, 2007, 4653.
56 H. Mochizuki, T. Yokoi, H. Imai, R. Watanabe, S. Namba, J. N. Kondo and T. Tatsumi, *Microporous Mesoporous Mater.*, 2011, **145**, 165.
57 M. Conte, J. A. Lopez-Sanchez, Q. He, D. J. Morgan, Y. Ryabenkova, J. K. Bartley, A. F. Carley, S. H. Taylor, C. J. Kiely and K. Khalid, *Environ. Sci. Technol.*, 2012, **2**, 105.
58 L. Narasimhan, J. Thybaut, G. Marin, J. Denayer, G. Baron, J. Martens and P. Jacobs, *Chem. Eng. Sci.*, 2004, **59**, 4765.